Long-range predictability in the tropics

Part I: Monthly averages

Thomas Reichler and John O. Roads

Scripps Institution of Oceanography

University of California San Diego, 9500 Gilman Dr., La Jolla, CA 92093-0224,

Correspondence to: John O. Roads (jroads@ucsd.edu)

Draft from Monday, March 10, 2003

Table of Contents

Abstract

The sensitivity of monthly mean tropical atmospheric forecasts to initial and boundary conditions during boreal winter is described. Five ensemble experiments were performed with an atmospheric general circulation model, forced with different combinations of initial and boundary conditions. The experiments were verified under the perfect model assumption. Boundary forcing was the main contributor to tropical predictability. Using persisted instead of observed boundary conditions led to lossof skill after 3 weeks. At lead times out to one season, the model appeared to perform considerably better when good initial conditions were provided. Regions of largest predictability were Indonesia and the central Pacific Ocean. The good predictability over the Pacific was related to ENSO, whereas that over Indonesia was strongly related to the large persistence of tropical divergent flow. It is suggested that the long persistence time scale could be related to a positive feedback of large-scale convective anomalies. The results show that good observations in the tropics are needed, and that good initial conditions should be used for long-range numerical predictions.

1. Introduction

The skill of numerical weather prediction models in forecasting the tropics at short to long ranges has always tended to lag that in the mid-latitudes (Kanamitsu, 1985; Reynolds et al., 1994). Forecasting tropical variations is not only complicated by the lack of good observations, but also by the relative complexity of tropical dynamics, which are governed by fundamentally different principles than the extratropics. Outside the tropics, quasi-geostrophic theory provides a relatively simple theoretical framework for an overall understanding of large-scale motions. In the tropics, pressure gradients and the Coriolis parameter are too small for motions to be in geostrophic balance. Other effects like friction or diabatic heating become important. The dominant energy source in the tropics is latent heat release associated with precipitation from convective cloud systems. The realistic parameterization of such systems represents a challenge for current numerical models.

This paper is focused on predictability of monthly averages, and therefore covers intraseasonal to interannual time ranges. The monthly time scale has not received much attention in recent studies of tropical predictability, which have focused more on the intraseasonal or Madden-Julian Oscillation (MJO; Madden and Julian, 1994). Most MJO related variability, however, is removed by taking monthly averages. Despite this separation of time scale it should be noted that MJO effects may still have some influence on monthly means. This is because the MJO exhibits variability on a very broad spectrum, which may also include periods longer than 60 days. In a companion paper (Reichler and Roads, 2003b), we investigated tropical predictability in relation to the MJO, and found that initial conditions are crucial for predicting this phenomenon correctly, but that there exists also an important response to external SST forcing.

The goal of this study was to examine the spatial and temporal structure of tropical predictability and its sensitivity to initial and boundary conditions. At the monthly time scale the effects of both initial and boundary conditions are important. This was shown recently by Reichler and Roads (2003a, thereafter referred to as RR). RR found that in the tropics, initial conditions dominated a numerical forecast during the first 3 weeks, and that only thereafter boundary conditions were more important. This relatively long time scale was surprising, since it is generally believed that the tropics are dominated by boundary forcing, and that initial conditions are unimportant (e.g. Shukla, 1998). This prompted further analysis, aimed at investigating the predictability of the tropics, and at finding the physical mechanisms behind the large sensitivity to initial conditions. As we will see, the tropical atmosphere is actually very slow in responding to changes in boundary conditions, particularly in areas, which are far away from the main forcing regions.

At what time scale does the tropical atmosphere respond to changes in the underlying forcing, and how sensitive are tropical forecasts to uncertainties in the description of the underlying ocean? These questions are not only relevant for coupled forecasting systems, but also for simpler ocean predictions. Persisted SSTs, for example, are regarded as good alternative to more expensive dynamical ocean forecasts on time scales out to three months (e.g., Mason et al., 1999; Roads et al., 2001). In this context, it is important to find out at what lead time and over which regions the added uncertainty introduced by using persisted SSTs weakens the skill of tropical forecasts.

This work is based on 5 ensemble experiments with an atmospheric general circulation model (AGCM). Each experiment was forced with different types of initial and boundary conditions, so that we were able to determine their individual contribution to

predictability. The experiments were designed to overcome several limitations posed by observations. Ensembles (10-20 members) of integrations were performed for many different years. By using the ensemble approach, unpredictable noisy components were separated from the various signals. Idealized combinations of initial and boundary conditions were prescribed in order to measure individual and cumulative contributions of each to predictability. These results also provided information about the upper predictability limit in the tropics.

In section 2, we briefly describe the model, experiments, and analysis technique used for this study. In section 3 we present a short discussion of the model's climatology in comparison with observational data. Section 4 discusses the temporally and spatially varying character of predictability using different initial and boundary conditions. Section 5 investigates further the long initial condition memory, and discusses its spatially varying character. Summary and conclusions are provided in section 6.

2. Methodology

a. Model experiments

The AGCM used for this study was the National Centers for Environmental Predictions (NCEP) seasonal forecasting model (e.g., RR; Kanamitsu et al., 2002) at T42 resolution with 28 vertical levels. Table 1 summarizes the 5 experiments of this study, which were carried out for 22 winter seasons (1979 to 2000). All simulations were started on December 15th and ran continuously through the end of the following March, a period which is simply designated as winter. The simulations were global, and initial and boundary conditions were modified globally. However, in the analysis presented here, only the local responses in the tropics were examined. The ensemble size was 20 for the control

simulation “ICBC”, and 10 for all other experiments. Members of one ensemble were forced with identically evolving boundary conditions, but were started from slightly different initial conditions. These initial conditions were derived from one of the 2 base runs or from reanalysis and perturbed by breeding (Toth and Kalnay, 1997). The two continuous AMIP-type base runs were carried out first. Run BASE-O was forced with observed global SSTs and sea ice, while BASE-C was forced with climatological SSTs and sea ice. Fig. 1 presents characteristic features of tropical SSTs during January in terms of their climatological mean (a), their interannual standard deviation (b), as well as anomalies during El Niño Southern Oscillation (ENSO) cold (c) and warm events.

The 5 experiments are identified by specific acronyms, which indicate what type of initial (IC) and boundary conditions (BC) were used. The perfect experiment “ICBC” was forced with observed global SSTs and sea ice, and was started from anomalous initial conditions of BASE-O. This was equivalent to using “observed” initial conditions, but under a perfect model assumption. Experiment “IC” was designed to measure the effect of initial conditions on predictability. IC used the same initial conditions as ICBC, but was forced with climatological ocean and land boundary conditions. To study the effects of boundary forcing alone, experiment “BC” was started from randomly chosen “climatological” initial conditions from BASE-C, but forced with the same perfect boundary conditions as ICBC. Experiment “ICP” was started from the same initial conditions as ICBC, but used persisted ocean boundary conditions. The final experiment “iBC” was started from initial conditions by integrating ICBC for one whole year. These initial conditions have completely lost their memory from the previous year, but they are adjusted to the boundary forcing at the new initialization time. In this respect, experiment

iBC was comparable to an ensemble of continuous AMIP-type integrations, and to the current operational seasonal forecasting methodology at the International Research Institute (IRI). The motivation for iBC was to find out how much predictability might be lost by excluding the beneficial effects of synoptic scales in the initial conditions.

b. Analysis procedure

Each three dimensional flow field was decomposed into rotational and divergent velocity components $\boldsymbol{v}_\psi$ and $\boldsymbol{v}_\chi$. Consider the two scalars, stream function ψ and velocity potential χ, which are related to the velocity components by:

$$\boldsymbol{v} = \boldsymbol{v}_\psi + \boldsymbol{v}_\chi = \boldsymbol{k}\times\nabla\psi + \nabla\chi\,. \tag{1}$$

The rotational part $\boldsymbol{v}_\psi$ satisfies automatically the condition of non-divergence, and the divergent part $\boldsymbol{v}_\chi$ satisfies the condition of irrotationality. In the tropics, where the geostrophic force balance is not valid, the divergent component of the wind field is more useful to describe the flow. Consequently, this analysis concentrates on the divergent component of the tropical circulation. More precisely, we focus on the predictability of the velocity potential at 200 hPa (χ_{200}), which emphasizes large scale features of the divergent flow. To analyze the daily data, the climatological mean annual cycle was removed, and then 30 day running means were taken. A monthly average has a low-pass characteristic with a cut-off period of approximately 60 days, and therefore emphasizes low-frequency variability beyond the MJO band. The 15 additional days at the beginning and end of the time series, which were needed for the moving averages, were generated by fitting an autoregressive model of order 5 to the 107 day forecasts.

Predictability was expressed in terms of the correlation between a *prediction* and a *verification* data set. For the prediction data set, 10-member ensemble means of the experiment under consideration were used. The verification data were taken from single realizations of the control experiment ICBC. Each of the 20 members of ICBC was selected as verification, and the average was used as the final result. Two forms of correlation measurements were used: First, the *spatial* anomaly correlation (*AC*) over a specific region; second, the *temporal AC* between annual time series of the verification and prediction data set for the same lag. To make the differences between *AC* values more meaningful, we applied a Fisher Z transformation (e.g., Roads, 1988) to the *AC*s before adding or subtracting the *AC*s, and then again transformed back to normal correlations. One should also keep in mind that correlation coefficients are statistically significant only when they exceed certain values. At the 95% error level, the critical values for the temporal *AC* were about 0.35 for all years (n=22). In some of our analysis we excluded certain years, so that the critical values were correspondingly larger (e.g., 0.5 for n=14).

3. Observed and simulated tropical climate

To illustrate that the AGCM was able to simulate a reasonable climate and to capture the main features of the tropical circulation, we describe in this section some aspects of the climatology and interannual variability of experiment ICBC for January monthly means in comparison to reanalysis. January was chosen since much of this study was focused on this month. The climatology covered 22 years (1979-2000); for the simulation ICBC the average over all 20 ensemble members was taken. The interannual variability was calculated over all years and all individual members.

Figs. 2 and 3 compare the rotational and divergent part of the tropical circulation for reanalysis and model. The rotational velocity component (Fig. 2) shows that in the upper air of the inner tropics weak easterlies prevailed over the eastern hemisphere, and westerlies over the western hemisphere. At the surface, most of the inner tropics were dominated by moderate easterlies. The velocity over the southern Indian Ocean was very weak. All of these features are captured quite well by the model, although the differences in the stream functions revealed some differences between the two circulations. The most important was over the southern warm pool region, where the model showed at both levels a much stronger clockwise circulation regime than the reanalysis. The divergent part of the circulation shown in Fig. 3 revealed somewhat larger differences between the two data sets, especially for the location and strength of the main convective region over the warm pool. which had strong lower level convergence and upper level divergence. While the model simulated three distinct centers of maximum convection over the Indian Ocean, the warm pool region, and South America, the reanalysis did not show as clear a separation into three different regions. Moreover, the divergent circulation in the model was too strong over the dateline, and too weak over the Indian Ocean. In this context it is important to emphasize that the divergent circulation was not really observed. Thus, the divergent circulation depends largely on the cumulus convection parameterization of the used model. Since the reanalysis model and the current model used different schemes, differences in the divergent circulation are perhaps not surprising.

The interannual variability of χ_{200} (Fig. 4, left) of both the reanalysis and the AGCM had maximum variability over the Indian Ocean. However, variability was somewhat higher in the model than in the reanalysis. Again, it may well be that the

reanalysis underestimated the interannual variability, since the model of this study presumably uses a physically more realistic convection scheme than the reanalysis. The interannual variability of the stream function (Fig. 4, right) was also somewhat higher in the model than in the reanalysis. Nevertheless, the overall patterns of stream function variability agreed quite well.

Since tropical precipitation is strongly related to convective activity, this field represents another indirect assessment for the realism of the simulated divergent circulation. The climatology and interannual variability of precipitation for CMAP (Climate Prediction Center Merged Analysis of Precipitation: Xie and Arkin, 1997) and AGCM are shown in Fig. 5. The climatology (left panels) shows there is an overall similar structure between observations and simulations. The three observed centers of strong precipitation over the Indian Ocean, the warm pool region and South America are present in the model simulations. Also, the characteristic South Pacific convergence zone is simulated well. A large difference between model and observations was the precipitation amount: The model produced too much rainfall over South America, and too little rainfall over the Indian Ocean. Moreover, the shape of the rainfall maximum over the Indian Ocean was not perfectly simulated. There, the model exhibits a double inter tropical convergence zone (ITCZ) structure, whereas the observations reveal only one narrow band of precipitation near the equator. Note, however, that the rainfall amount distribution near the date line is about right, even though the velocity potential showed larger differences between reanalysis and simulations. The patterns of interannual variability of precipitation (right panels) were about the same as that of the rainfall amounts. The observations indicate a broad area of maximum variability over the Indian Ocean and around the date

line, and a secondary maximum over South America. The AGCM reproduced quite well these centers.

Even though the model did not reproduce exactly the observed atmosphere, it did seem to capture the basic patterns. Therefore, we think that the AGCM of this study is an adequate tool for the investigation of low-frequency predictability in the tropics.

4. Analysis of predictability

a. Lead time evolution

Consider first the evolution of predictability as a function of lead time. Predictability is measured by the spatial *AC* of daily low-pass filtered χ_{200} along the equator (10ºN to 10ºS). The spatial *AC* was calculated for each time step, ensemble member and year. Fig. 6 shows the lead time evolution of the *AC*s in daily increments from day 1 (Dec. 15th) out to day 107 (March 31st) for the five experiments. The left panel (a) shows the *AC* averaged over all 22 years (1979-2000), and the right panel includes only neutral to weak ENSO years. Neutral to weak ENSO years included all years from the 1979-2000 period except the strong ENSO years listed in Table 2.

The upper bound of predictability with this model is indicated by experiment ICBC (continuous line). Predictability is high at short lags because of the initial condition effect. After several weeks, the skill of the three experiments, which were forced with perfect boundary conditions (ICBC, iBC and BC), converge to the same value of about 0.7. This rather high predictability reflects the dominant role of boundary forcing in the tropics. Even when only neutral to weak ENSO years are included (right panel), the correlations for ICBC do not drop below 0.5. Hence, even in the absence of strong ENSO, boundary effects are still quite important. From the differences in correlations between ICBC, iBC

and BC the importance of initial conditions for tropical forecasts can be seen. It took about 40-50 days for simulation iBC to approach the same level of skill as ICBC. Experiment BC practically never reached the skill of ICBC, not even at the longest lead times. Furthermore, the correlations of iBC were consistently higher than those of BC. We recall that iBC comes from fully adjusted initial conditions, and BC comes from climatological initial conditions. This figure therefore indicates clearly that the tropical atmosphere adjust very slowly to changes in its boundary conditions, and that initial conditions are important in the tropics even at long lead times. Even initial conditions alone can produce considerable skill, as can be seen from the very slow approach of IC to zero skill. It took about 60 days until IC reached zero correlation. One way to measure the relative importance of initial and boundary conditions is by the time it takes for the skill of IC to intersect with that of BC. This time, which was on the order of 20-30 days for these experiments, indicates that the influence of boundary forcing was as important for long-range predictability as the decaying influence of initial conditions.

The relatively rapid loss in predictability for simulation ICP, which was forced by persisted boundary conditions, was rather surprising. After only 20 days, there existed substantial differences between the ICP and the ICBC predictions. Given the slow time scale of ocean SSTs, this means that even very subtle differences in boundary forcing might have large impacts on the atmospheric forecast. However, ICP never reached zero skill as simulation IC. This was probably due to the fact that ENSO related SST anomalies are usually well developed during December and persist throughout winter.

b. Interannual variations

The year to year variability of tropical predictability and how it was related to initial and boundary conditions is shown in Fig. 7. For each year and experiment, the spatial *AC* of the January monthly mean χ_{200} over the equatorial band (10ºN to 10ºS) is shown. January corresponds to forecast day 32 or week 3-6, since the experiments were initialized on December 15th. The years are arranged according to the correlations for experiment ICBC (black bars). Results for the other experiments (colored bars) are displayed as differences to ICBC. From the year to year breakdown one can see how important initial or boundary conditions were during specific years. From the large correlations of ICBC, iBC and BC during ENSO years it is quite clear how important ENSO related boundary forcing for tropical predictability was. Interestingly, during some ENSO years, the correlations for IC did not differ much from ICBC; during some non-ENSO years (e.g., 1995, 1982, 1994), IC had even higher correlations than BC. The correlations of ICP were in most cases close to ICBC. Only the years 1984, 1987 and 1994 had relatively large differences. Thus, at this lead time interval, persisted SSTs represented a relatively good choice as a boundary condition.

c. Spatial structure

The spatial structure of monthly mean predictability of χ_{200} over the tropical domain during January is shown in Fig. 8. Predictability was measured at each grid point by the temporal anomaly correlation between annual time series of a prediction and verification data set. Each time series consisted of January monthly mean fields of all 22 years (left panels), and of 14 neutral to weak ENSO years (right panels). During neutral to weak ENSO years, boundary effects were weaker, so that the more subtle initial condition

effects became more important. The perfect experiment ICBC had for all years (top left panel) rather high correlations. Two distinct predictability maxima with correlations of 0.8 and more can be seen over the Pacific Ocean and over the warm pool region. Areas of lowest predictability occurred over the continental areas of South America and Africa. Predictability of iBC and BC was lower than that of ICBC, demonstrating the impacts of not having perfect initial conditions. The loss in skill was particularly strong over the warm pool around 120°E, and over South America and the Atlantic. Consistent with different qualities in initial conditions, simulation BC exhibited smaller predictability than iBC. Simulation IC had much lower correlations than the boundary forced experiments, but over some regions, the memory of initial conditions was still strong enough to produce correlations of 0.5 and more. Interestingly, the maximum skill for simulation IC was located over the warm pool region, exactly where iBC and BC have maximum loss in skill. This indicates that initial conditions were particularly important for this region. The patterns of predictability of ICP were quite similar to iBC, but the loss in skill for experiment ICP was spatially more uniform.

The panels on the right hand side of Fig. 8 show predictability correlations during neutral to weak ENSO years. The correlations were generally smaller, although ICBC still had rather high correlations. The Pacific region, which was well predictable when averaging over all years (left panels), now had strongly reduced skill. This means that the good predictability over this region was strongly related to ENSO. On the other hand, predictability over the warm pool region, where the correlations were now maximum, depended to a much lesser extent on ENSO. Experiments iBC and BC had a strong loss in skill, which extended over larger areas than for all years. As seen before, initial conditions

were very important over the Indian Ocean. There, experiment IC had even better skill than iBC or BC. Maximum loss in skill for ICP was found over South America and to the east of Africa.

d. Time-space characteristics

Fig. 9 presents temporal correlations (1979-2000) of χ_{200} (top panels) and precipitation (bottom panels) along the equator (10°N to 10°S) as a function of lead time in a Hovmöller diagram. The data were low-pass filtered using 30 day running averages before the correlations were calculated. The results for experiment ICBC (left panels) are shown as absolute correlations, and the remaining panels show differences in correlation to ICBC. Note that the correlations at day 32 correspond to the monthly mean of January, which was discussed in the previous section. For χ_{200} (top panels), simulation ICBC had two predictability maxima over the Pacific and Indian Oceans, which sustained for very long time. One can see from simulation BC, and to some extent also from iBC, over which areas imperfect initial conditions led to reduced predictability at long lead times. The most affected area was the eastern hemisphere, and least sensitive was the region around the date line. Interestingly, the most persistent errors were located over regions which were far away from the date line. Simulation IC had the largest loss in skill over the central Pacific. The loss in skill over the Indian Ocean was smallest, and there the correlations were statistically significant (>0.3) out to 50 days. Thus, to some extent the predictability pattern of IC was just the inverse of BC. Simulation ICP shows that the errors introduced by using persisted boundary conditions evenly affected all regions. The largest error growth occurred over the western Indian Ocean and the Atlantic.

The bottom panels of Fig. 9 display the associated predictability for precipitation. This allows a direct comparison of the predictability structure of the upper atmosphere with that at the surface. Precipitation is characterized by high temporal and spatial variability, which is difficult to predict. Therefore, it is not surprising that the correlations for precipitation are smaller than those for χ_{200}. Nevertheless, the overall patterns of predictability for the two variables are quite similar. Surprisingly, precipitation is more predictable than χ_{200} over some areas. Also, for precipitation simulations iBC and BC have lower skill than ICBC even at very long lead times. Note the predominantly negative differences to ICBC. Similarly as before, iBC has somewhat higher correlations than BC. Simulation IC reveals that initial conditions alone produce useful precipitation forecasts only at short leads out to about 20 days. Overall, this comparison showed that initial conditions impact upper air variables as well as surface quantities, and that the findings from upper air quantities were, to some extent, applicable to surface variables.

5. The role of initial conditions

Our model results indicated that the tropical atmosphere responds relatively slowly to changes in SSTs, and that it remembered its initial conditions for several weeks. This effect seemed to be particular strong over the Indian Ocean, and it was relatively small over the Pacific Ocean. In this section, we explore the physical mechanisms behind this long initial condition memory. The analysis was focused on the two experiments ICBC and IC, and we will show monthly means during January, which again corresponded to forecasts for weeks 3-6.

a. Persistence of tropical flow

We noted before that even during years with strong boundary forcing, predictability from using just initial conditions was quite high (see Fig. 7), which indicated that the divergent circulation of the tropical atmosphere was persistent. To further examine this persistent behavior, we present the time evolution of χ_{200} for two specific years. The time-longitude diagrams in Fig. 10 show the temporal evolution of the ensemble mean anomalies for experiments ICBC, IC and BC along the equator. During 1982, simulation ICBC (top left panel) had a strong positive anomaly over the Indian ocean, which persisted for the whole 107 day long forecasting period. Because 1982 was not an ENSO year boundary forcing alone cannot fully explain this phenomenon. The same persistent anomaly appears in simulation IC (top middle panel). Another very persistent behavior occurred during 1985 (bottom panels). Simulation ICBC was characterized by very long lasting negative anomalies over the Indian Ocean, and positive anomalies over the Pacific. These anomalies were consistent with the ENSO cold event that happened during this year. Colder than normal SSTs over the Pacific led to reduced convective activity and to anomalous upper level convergence, shown here by the positive χ_{200} anomalies over the western Pacific. The negative anomaly over the Indian Ocean was also a response to the cold event, and was related to the indirect coupling between individual cells of the zonal and meridional overturning circulation. In simulation IC, the negative anomaly over the Indian Ocean persisted for many weeks, whereas that over the Pacific disappeared much faster. This East-West difference was similar to what had already been noted before.

b. Case study

In this section, we describe in detail the 3-dimensional structure of the divergent circulation from the two experiments ICBC and IC. First, the climatological mean of the model's divergent circulation is presented. Fig. 11 shows different cross sections from simulation ICBC during January. The top panel shows a contour map in the longitude-latitude plane of vertical velocity at 400 hPa, which indicates the preferred locations for deep convective activity. The vectors represent the direction and strength of the horizontal divergent mass flux, which was calculated following Trenberth et al. (2000). There are 3 distinct centers of tropical convection. The centers of maximum convective activity were located at about 10°S, where maximum SSTs could also be found (see Fig. 1). The height-latitude plot (middle panel) was centered over the convective region over the warm pool and indicates zonal averages from 120°E to 120°W, which illustrates the meridional overturning circulation (Hadley cell). The Hadley cell was much stronger over the northern than over the southern hemisphere. The height-longitude plot (bottom panel) shows the divergent flow in the zonal direction along the equator. The main convective area over the warm pool was the source for 2 zonal overturning cells, one going towards the east (Walker cell), and one in the opposite direction. The other 2 areas of strong convection, one over the western Indian Ocean and one over South America, had 2 zonal overturning cells. This led to a total of 6 cells along the equator with alternating circulation.

Next, consider the anomalous circulation of ICBC and IC during specific years in comparison with the climatological mean. Again, we selected the January mean circulation of three strong ENSO cold events (1985, 1989 and 1998) and averaged them to one composite. The choice of these three years was motivated by the fact that their SST forcing

patterns were similar. This caused similar atmospheric responses, and meaningful composites could be constructed. Fig. 12 shows the composite anomalies from simulation ICBC. The curve at the bottom of Fig. 11 shows that SSTs over broad areas of the Pacific were colder than normal. The maximum atmospheric response to these SST anomalies was located over the date line, with strong anomalous downward motion and upper-level convergence. The anomalous downward motion was compensated by anomalous upward motion over most other areas. The indirect coupling of the divergent circulation led to anomalies in all six zonal overturning cells. Those cells, which were close to the forcing region had decreased intensity, whereas the more remote ones had an intensification.

Fig. 13 presents the circulation anomalies for experiment IC. Even though simulation IC was forced with climatological SSTs, many of the ICBC circulation anomalies were still present. More specifically, the anomalies over the eastern hemisphere were quite well preserved, whereas the circulation over the western hemisphere was close to climatology. The anomalies over the east could only originate from the initial conditions from experiment IC, which must have persisted throughout the forecast despite the climatological boundary forcing. Imposing climatological SSTs to an atmosphere which was adjusted to a cold event was similar to warming up the SSTs. We originally thought this would increase the convective activity over the warm pool and bring the circulation back to climatology. Instead, the circulation returned only very slowly. We also investigated composites of simulation IC from warm ENSO years (not shown). Curiously, a similar delayed response to the now cooler than normal SSTs could not be found. Instead, the January mean circulation of simulation IC during warm ENSO years was almost everywhere close to the climatological mean.

c. East-west contrast

Our results indicated that the persistence time scale over the Pacific Ocean was shorter than over the Indian Ocean, and that therefore initial condition predictability was more effective over the eastern hemisphere. Furthermore, the response of the circulation seemed to be asymmetric with respect to the SST forcing, since during cold ENSO years the persistence of simulation IC was larger than during warm ENSO years. These features could be more clearly seen when predictability was calculated separately for the two hemispheres, and separately for ENSO warm, cold and neutral years. Fig. 14 shows the lead time evolution of the spatial anomaly correlation of low-pass filtered χ_{200} for the five experiments, calculated for the two hemispheres and the different years. Since the *AC*s were averaged only over few years, the results were somewhat noisy. During ENSO warm events (top panels), the perfect run ICBC had better predictability over the west than over the east. Initial conditions were more important over the east, as can be seen from the slow increase in skill for BC and iBC, and from the relative slow descent of IC to zero skill. During cold ENSO years (middle panels), initial conditions were even more important over the east, whereas they played only a minor role over the west. During neutral to weak ENSO years (bottom panels), ICBC had higher correlations over the east, but initial conditions seemed to be important over both hemispheres. Experiment ICP shows an interesting asymmetric behavior between east and west. During warm and cold ENSO years, the loss in predictability from using persisted SST boundary conditions was clearly larger over the eastern hemisphere. This indicated that over the Pacific Ocean persisted boundary conditions are a better approximation to the real SSTs than over the Indian

Ocean. During neutral years, the loss in skill is considerable for ICP over both hemispheres.

Observed variability of convection is largest over the Indian Ocean region (e.g., Salby et al., 1994). In the model, variability of the tropical divergent circulation also had a characteristic east-west difference, as demonstrated by Fig. 15. It shows the internal variability component from filtered χ_{200} for simulations ICBC and IC. The internal variability was calculated from the spread of individual members around the ensemble mean at individual dates. It therefore did not include interannual variability due to external forcing. The variability was about twice as strong over the eastern than over the western hemisphere, presumably because of stronger variations in convective activity over the East. The interannual variability revealed already such asymmetry, as was shown before for January monthly means of χ_{200} (Fig. 4) and precipitation (Fig. 5). The exact reasons for this contrast are unclear, but may be related to different SST conditions over the Pacific and Indian Oceans. The year to year variability of tropical SSTs (Fig. 1b) was large (<2.0°K) over the central equatorial Pacific, but quite small (<0.2°K) over the remaining ocean areas. Moreover, the mean SST conditions (Fig. 1a) over the central and eastern equatorial Pacific and over the Atlantic were relatively cool (<27°C), whereas the warm pool region and the whole Indian Ocean were relatively warm (>27°C). This SST difference may have had important implications for the development of deep convection, since it is known that the strength of convection is coupled to the underlying SSTs. Observations, for example, have concluded that little convective activity takes place over SSTs colder than 26-27°C (Graham and Barnett, 1987). Apparently, the strong east-west temperature gradient over the Pacific led to the development of one large and stable east-

west overturning circulation (Walker cell, see Fig. 11b), which was controlled by strong interannual SST variations due to ENSO. By contrast, the Indian Ocean and the warm pool region were warm everywhere, which means that convection was spatially less confined. Effects from boundary forcing were also small since the SST variability was small. Therefore, large scale convective anomalies could develop more freely than over the Pacific Ocean region. This may explain why the intraseasonal variability over the eastern hemisphere was larger than over the western hemisphere. Finally, since these convective anomalies seemed to have a slow time scale, the initial condition effect seemed to be more effective over the East.

We also explored the statistical relationships between initial condition predictability, atmospheric activity, and intensity of SST forcing. The initial condition predictability was measured by the time T until the spatial anomaly correlation of low-pass filtered daily χ_{200} of IC verified against ICBC (see Fig. 14) fell below a (arbitrary) value of 0.4. Atmospheric activity was measured by the spatial standard deviation of low-pass filtered χ_{200} of experiment IC at the beginning of the forecast (t=0). The intensity of the SST forcing was derived from the spatial standard deviation of observed SST anomalies averaged from time 0 to time T. Eastern and western hemispheric data from simulation IC were analyzed separately.

Fig. 16 shows the results in the form of scatter plots. Each of the 22 crosses represent values for one year. Warm and cold ENSO years are shown by red and blue crosses, respectively. The top panels show the relationship between atmospheric activity and initial condition predictability from experiment IC. Over the eastern hemisphere, this relationship is positive, meaning that strong anomalies in χ_{200} at the beginning of

the forecast led to better forecasts. The correlation of around 0.7 is statistically significant, and reflects the persistent nature of the eastern hemisphere. Over the West, this relationship is just the opposite; in other words, the stronger the atmospheric anomalies at the beginning, the lower the predictability from initial conditions. In particular strong ENSO years led to low forecast skill from initial conditions. Presumably, this occurred because the atmosphere over the West was dominated by boundary forcing from the Pacific. This can also be seen in the bottom panel on the right. Over the eastern hemisphere, the atmospheric activity was almost unrelated to the SST conditions underneath (bottom left panel). Also, the SST conditions over the central Pacific were only loosely related to the atmospheric activity over the East, since as many ENSO as non-ENSO years are associated with increased atmospheric activity.

6. Summary and Discussion

This study examined the sensitivity of monthly averaged forecasts in the tropics to initial and boundary conditions during boreal winter at lead times from one day out to one season. A numerical model was used to conduct five experiments, each with different combinations of initial and boundary conditions. The experiments were verified under the perfect model assumption to eliminate model related errors. A comparison with observational data showed that the climatology and interannual variability of divergent and rotational components of the flow and the associated precipitation were simulated quite realistically by the model. When perfect boundary conditions were provided, the correlations of monthly averages at long leads were about 0.7 when years with strong ENSO forcing were included, and about 0.5 when those years were excluded. Skill maxima were found over the central Pacific Ocean and over the warm pool region.

Overall, the model showed high sensitivity to the kind of initial conditions - at all lead times and over all regions. Initial conditions were most important over the Indian Ocean and warm pool region. Predictability over the Pacific Ocean, on the other hand, was mostly connected to ENSO related boundary forcing. Using persisted instead of perfect SST boundary conditions started to have negative effects on predictability after only 2-3 weeks, and led to considerable loss in skill at longer lead times. All regions were affected, but the largest loss in skill was found over the Atlantic Ocean and the eastern Indian Ocean region. The above conclusions also hold for the sensitivity of precipitation forecasts to initial and boundary conditions. Practical predictability, where real data were used as input and as verification, was lower than the perfect model skill; the lack of good observations and the difficulties in realistically describing the diabatic heating terms are likely candidates, which contributed to this decreased skill.

Special attention was devoted to the question of why tropical forecasts were so sensitive to initial conditions, and why this mainly occurred over the Indian Ocean. It was shown that the long initial condition memory was closely related to the persistent behavior of divergent circulation. From initial conditions alone, the tropical atmosphere was able to remember the full 3-dimensional anomalous circulation of strong ENSO cold events for many weeks. A corresponding effect during warm events could not be found. These results suggest the following picture: The divergent flow over the western hemisphere, and in particular over the Pacific Ocean, is dominated by interannual SST variations from ENSO, and intraseasonal variability is relatively small. Over the eastern hemisphere, and here mainly over the Indian Ocean, the intraseasonal variability is much higher. The reasons for this are not fully understood, but we speculated that the structure of the underlying ocean

SST was related to it. Over the Indian Ocean, the SST variability was much smaller, so that boundary forcing effects were less important. Remote effects from slowly evolving ENSO events were only one factor forcing the divergent circulation. More important, the ocean were warm enough everywhere for the development of large scale convective anomalies. The persistent character of these anomalies was responsible for the long term memory of initial conditions over the Indian Ocean.

We speculate that the long persistence time scale of tropical convection is related to forcing from the large scale wind field. Several observational and modeling studies (e.g., Lau et al., 1994; Lau et al., 1997; Tompkins and Craig, 1999) showed that convection was insensitive to changing SSTs in the absence of large scale flow. Conversely, this means that convection could be very sensitive to large scale wind forcing. For example, anomalous upward motion favors convective activity, which in turn may feed on itself and create further upward flow. Once a large scale circulation anomaly is established, it creates its own favorable conditions through the suppression or activation of convection, and therefore remembers itself for a long time. Another hint comes from the response with respect to the sign of the forcing. The long term memory of initial conditions was mostly active during cold events, or during years with little or no forcing. During warm years, the circulation returned much faster to the climatological state. This indicates the existence of an asymmetry in the response of the circulation to SST forcing, indicating convection was more sensitive to cold than to warm SST anomalies. Cool SSTs can effectively reduce convection, but warm SSTs do not immediately cause more convection. This may again be related to an inherently positive feedback of tropical convection, in the sense that

preexisting convection creates favorable conditions for further convection. This feedback may be part of or be amplified by the aforementioned effect of large scale wind forcing.

There were strong qualitative similarities between the results of this study and a recent paper from Tompkins (2001). In a comparable experimental design, he investigated the response of a cloud-resolving model to sudden changes of cold and warm SSTs. Even though this was a somewhat different model, he found a surprisingly similar result: Tropical convection died out quickly over cool SSTs, but convection did not spontaneously flare up over warm SSTs. Instead, convection propagated slowly toward the warm anomaly at a time scale of several weeks. Tompkins (2001) suggested that a organizational positive feedback between water vapor and convection would make future convection likely to occur at locations where convection already exists. That is, the presence of convection moistens the atmosphere, making it favorable for future convection. Dry air, on the other hand, inhibits the break out of convection even in the presence of warm SSTs. In order for convection to occur, moisture needs to be advected from remote areas. He concluded that the slow advective adjustment timescale of water vapor acts like a memory in tropical dynamical circulations.

Despite the similarities of these two modeling studies, we want to emphasize that it is still unclear whether these results can be observed in nature. It is particularly important to note that the initial condition effects were closely related to convection, and therefore to the kind of cumulus convection parameterization used. Since modern AGCMs are beginning to use the same scheme as this model (RAS), they are all likely to show a similar behavior. Thus, independent of the question of real or artefact, this emphasizes the need for good observations and initial conditions in the tropics. Ultimately, this will not

only improve tropical forecasts, but will have also positive impacts on extratropical long-range predictions.

Acknowledgements: We thank M. Kanamitsu for many insightful discussions and for his help with the model. Funding for this research was provided by a cooperative agreement with NOAA (NA77RJ0435 and NA17R1231) and NASA grant NAG8-175. The views expressed herein are those of the authors and do not reflect the views of NOAA and NASA. We thank the Maui High Performance Computing Center (MHPCC) and the San Diego Supercomputing Center (SDSC) for providing computing time for some of the experiments. This work is part of the PhD thesis of T. Reichler.

References

Graham, N. E. and T. P. Barnett, 1987: Sea surface temperature, surface wind divergence and convection over tropical oceans. *Science,* **238,** 657-659.

Kanamitsu, M., 1985: A study of the predictability of the ECMWF operational forecast model in the tropics. *J Meteorol Soc Japan,* **63,** 779-804.

Kanamitsu, M., et al., 2002: NCEP dynamical seasonal forecast system 2000. *Bulletin of the American Meteorological Society,* **83,** 1019-1037.

Lau, K. M., H. T. Wu, and S. Bony, 1997: The role of large-scale atmospheric circulation in the relationship between tropical convection and sea surface temperature. *J Climate,* **10,** 381-392.

Lau, K. M., C. H. Sui, M. D. Chou, and W. K. Tao, 1994: An Inquiry into the Cirrus-Cloud Thermostat Effect for Tropical Sea Surface Temperature. *Geophys Res Lett,* **21,** 1157-1160.

Madden, R. A. and P. R. Julian, 1994: Observations of the 40-50-Day Tropical Oscillation - a Review. *Mon Weather Rev,* **122,** 814-837.

Mason, S. J., L. Goddard, N. E. Graham, E. Yulaeva, L. Q. Sun, and P. A. Arkin, 1999: The IRI seasonal climate prediction system and the 1997/98 El Nino event. *Bull Amer Meteorol Soc,* **80,** 1853-1873.

Reichler, T. and J. O. Roads, 2003a: The role of boundary and initial conditions for dynamical seasonal predictability. *Nonlinear Proc Geophys***,** (in press).

Reichler, T. and J. O. Roads, 2003b: Long range predictability in the tropics. Part II: 30-60 day variability. *J Climate***,** (submitted).

Reynolds, C. A., P. J. Webster, and E. Kalnay, 1994: Random Error Growth in NMC Global Forecasts. *Mon Weather Rev,* **122,** 1281-1305.

Roads, J. O., 1988: Lagged average predictions in a predictability experiment. *J Atmos Sci,* **45,** 147-162.

Roads, J. O., S. C. Chen, and F. Fujioka, 2001: ECPC's weekly to seasonal global forecasts. *Bull Amer Meteorol Soc,* **82,** 639-658.

Salby, M. L., H. H. Hendon, and R. R. Gacia, 1994: Intraseasonal Behavior of Clouds Temperature, and Motion in the Tropics. *J Atmos Sci*, **51,** 3365-3365.

Shukla, J., 1998: Predictability in the midst of chaos: A scientific basis for climate forecasting. *Science,* **282,** 728-731.

Tompkins, A. M., 2001: On the relationship between tropical convection and sea surface temperature. *J Climate*, **14,** 633-637.

Tompkins, A. M. and G. C. Craig, 1999: Sensitivity of tropical convection to sea surface temperature in the absence of large-scale flow. *J Climate,* **12,** 462-476.

Toth, Z. and E. Kalnay, 1997: Ensemble forecasting at NCEP and the breeding method. *Mon Weather Rev*, **125,** 3297-3319.

Trenberth, K. E., D. P. Stepaniak, and J. M. Caron, 2000: The global monsoon as seen through the divergent atmospheric circulation. *J Climate*, **13,** 3969-3993.

Xie, P. P. and P. A. Arkin, 1997: Global precipitation: A 17-year monthly analysis based on gauge observations, satellite estimates, and numerical model outputs. *Bulletin of the American Meteorological Society,* **78,** 2539-2558.

Table and Figure Captions

Table 1: Boundary and initial conditions, ensemble size and simulation period for each experiment. Winter refers to December 15th – March 31st of the following year. 'rndm' indicates randomly chosen initial conditions, 'clim.' indicates climatological boundary conditions, 'cont.' indicates continuous base run over all years, 'obs.' means observed (i.e. reanalysis-1), and 'r-2' indicates NCEP/DOE reanalysis-2.

Table 2: Classification of strong ENSO years during January 1979-2000.

Fig. 1: (a) Climatological mean (1979-2000) SST conditions during January; (b) interannual standard deviation of SST during January; SST anomalies during composite ENSO cold (c) and warm (d) events; all units are in ºC.

Fig. 2: January climatology (1979-2000) of stream function ψ (contours) and rotational velocity components (vectors) from NCEP/NCAR reanalysis (top) and model simulation ICBC (bottom). Left panels are for lower troposphere (850 hPa), and right panels are for upper troposphere (200 hPa). Units are $10^6\,m^2s^{-1}$.

Fig. 3: As Fig. 2 but for velocity potential χ and divergent velocity components.

Fig. 4: Interannual standard deviation of January monthly mean velocity potential χ (left) and stream function ψ (right) at the 200 hPa level from NCEP/NCAR reanalysis (top) and model simulation ICBC (bottom). The base period is 1979-2000. Units are $10^6\,m^2s^{-1}$.

Fig. 5: Climatology (left panels) and interannual standard deviation (right panels) of January monthly mean precipitation from CMAP (top) and model simulation ICBC (bottom). The base period is 1979-2000. Units are mm/d.

Fig. 6: Lead time evolution of spatial anomaly correlation from low-pass filtered equatorial χ_{200} (10ºN to 10ºS). (a) shows averages over all years, and (b) shows averages over neutral to weak ENSO years. Vertical axis denotes correlation. See Table 1 for definitions of ICBC, iBC, BC, IC and ICP.

Fig. 7: Interannual variations of spatial anomaly correlations during January, derived from monthly mean equatorial χ_{200} (10ºN to 10ºS). Results for ICBC show absolute correlations, and other experiments show differences to ICBC. Cold (warm) ENSO years are shown by blue (red) year numbers. Vertical axis denotes correlation.

Fig. 8: Temporal anomaly correlations of January mean χ_{200} assuming perfect model. Left panels are for all 22 years from 1979-2000, and right panels are for neutral to weak ENSO years. See Table 1 for definitions of ICBC, iBC, BC, IC and ICP.

Fig. 9: Hovmöller diagram of temporal anomaly correlation (1979-2000) of monthly mean data along the equator (10°N-10°S). Top panels are for χ_{200}, and bottom panels are for precipitation. ICBC shows absolute correlations, and the other experiments show differences with respect to the ICBC. See Table 1 for definitions of ICBC, iBC, BC, IC and ICP.

Fig. 10: Temporal evolution of low-pass filtered χ_{200} during winter 1982 (top) and 1985 (bottom). Shown are ensemble mean anomalies along the equator (10°N-10°S) from simulation ICBC (left), IC (middle), and BC (right). Units are $10^6\ m^2s^{-1}$.

Fig. 11: Climatological mean (1979-2000) divergent circulation of simulation ICBC during January. Contours show vertical velocity in mm/s, and vectors show mass flux in $kg\ m^{-2}\ s^{-1}$. Shown are vertical velocity at 400 hPa and mass flux at 200 hPa in the XY-plane (top), zonal averages from 120°E-120°W in the YZ-plane (top-middle), meridional averages from 0-20°S along the equator (bottom-middle) and associated SSTs in °C (bottom). The cross sections use pressure in hPa as vertical coordinate (y-axis).

Fig. 12: As Fig. 11 but composite anomalies of 1985, 1989 and 1998 for simulation ICBC.

Fig. 13: As Fig. 11 but for simulation IC.

Fig. 14: Lead time evolution of spatial *AC*s of χ_{200} along the equator (10ºN to 10ºS), calculated separately for the eastern (0-180º) (left) and western (180º-360º) (right) hemisphere, and for warm (top), cold (middle) and neutral to weak ENSO years (bottom). See Table 1 for definitions of ICBC, iBC, BC, IC and ICP.

Fig. 15: Internal variability of filtered χ_{200} (10°N-10°S), averaged over day 40-106 and all 22 years (1979-2000). Units are $10^{12}\ m^4s^{-2}$.

Fig. 16: Relationship between year to year variations in SST forcing (K), atmospheric activity ($10^6\ m^2s^{-1}$), and initial condition predictability (days). Left panels are for eastern hemisphere (0º-180º), and right panels are for western hemisphere (180º-360º). Text in the

upper left corner shows correlation between the quantities. Red (blue) x's indicate years with ENSO warm (cold) events.

Table and Figures

Table 1: Boundary and initial conditions, ensemble size and simulation period for each experiment. Winter refers to December 15th – March 31st of the following year. 'rndm' indicates randomly chosen initial conditions, 'clim.' indicates climatological boundary conditions, 'cont.' indicates continuous base run over all years, 'obs.' means observed (i.e. reanalysis-1), and 'r-2' indicates NCEP/DOE reanalysis-2.

	boundary conditions		*initial conditions*				
name	*ocean*	*land*	*atmosphere*	*land*	*size*	*period*	*years*
BASE-O	observed	model	obs. 1/1/48	obs. 1/1/48	1	cont.	1948-2000
BASE-C	clim.	model	obs. 1/1/48	obs. 1/1/48	1	cont.	1948-2024
ICBC	observed	model	BASE-O	BASE-O	20	winter	1979-2000
ICP	persisted	model	BASE-O	BASE-O	10	winter	1979-2000
IC	clim.	r-2 clim.	BASE-O	-	10	winter	1979-2000
BC	observed	model	BASE-C rndm.	BASE-C rndm.	10	winter	1979-2000
iBC	observed	model	ICBC, 1 yr lag	ICBC, 1 yr lag	10	winter	1980-2001

Table 2: Classification of strong ENSO years during January 1979-2000.

event	*January*
cold	1985, 1989, 1999, 2000
warm	1983, 1987, 1992, 1998

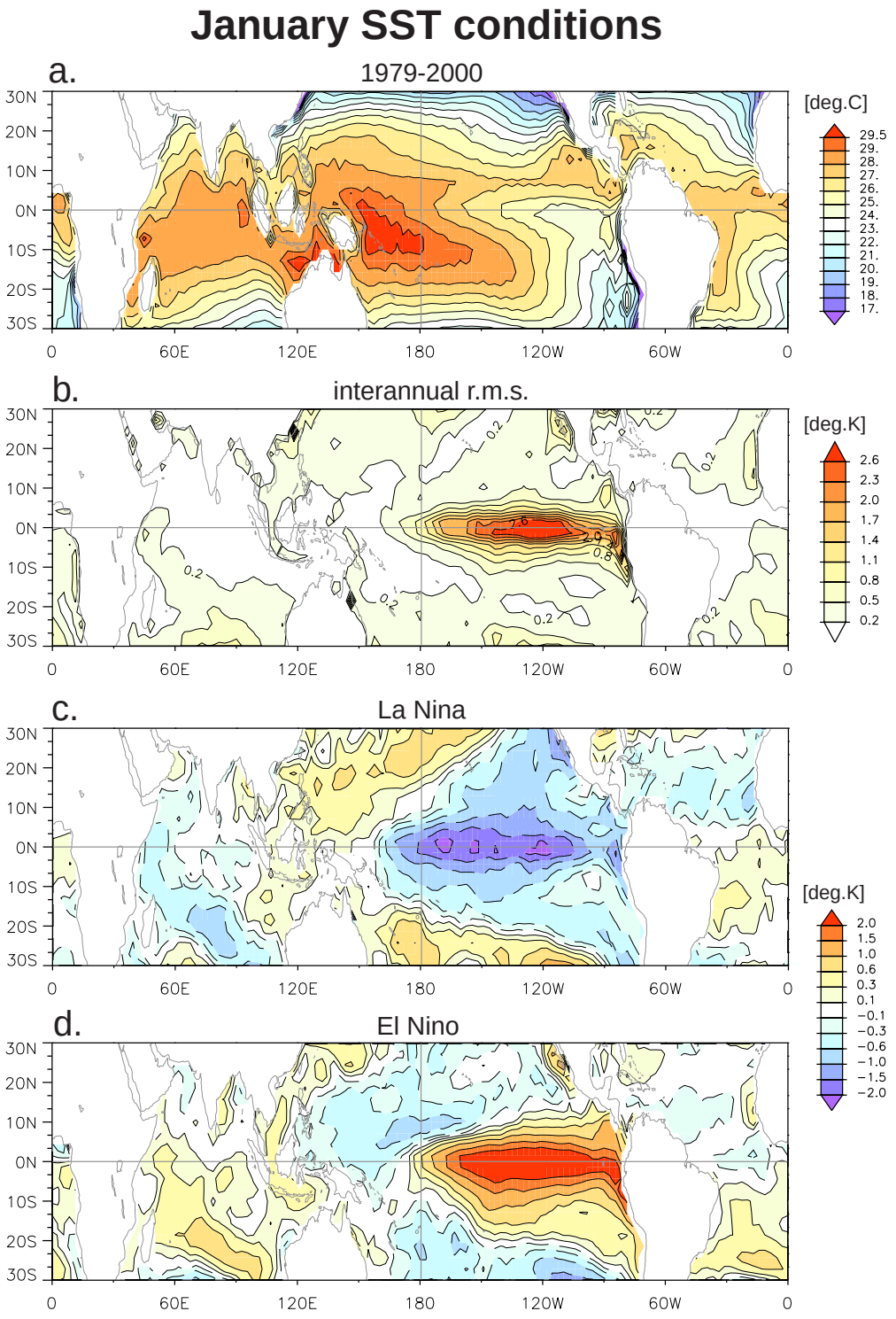

Fig. 1: (a) Climatological mean (1979-2000) SST conditions during January; (b) interannual standard deviation of SST during January; SST anomalies during composite ENSO cold (c) and warm (d) events; all units are in ºC.

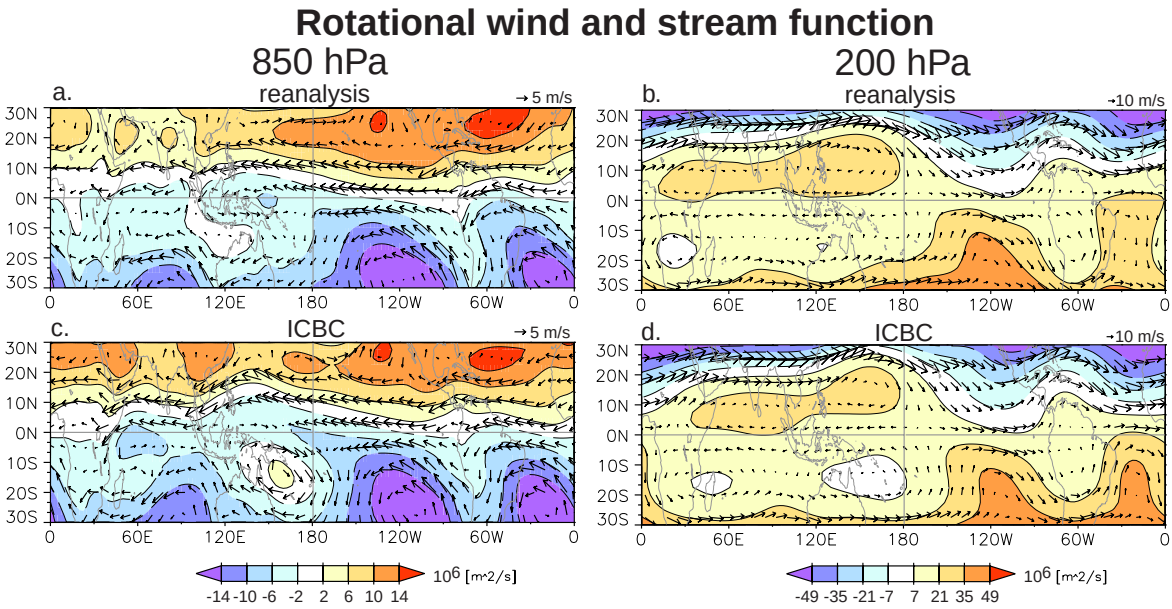

Fig. 2: January climatology (1979-2000) of stream function ψ (contours) and rotational velocity components (vectors) from NCEP/NCAR reanalysis (top) and model simulation ICBC (bottom). Left panels are for lower troposphere (850 hPa), and right panels are for upper troposphere (200 hPa). Units are 10^6 m^2s^{-1}.

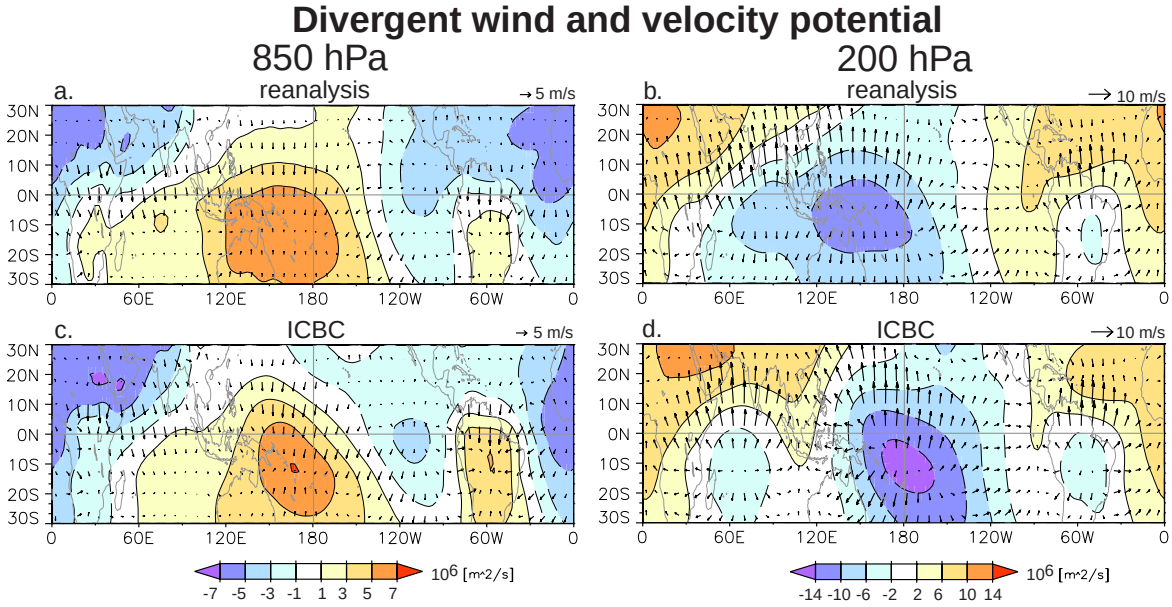

Fig. 3: As Fig. 2 but for velocity potential χ and divergent velocity components.

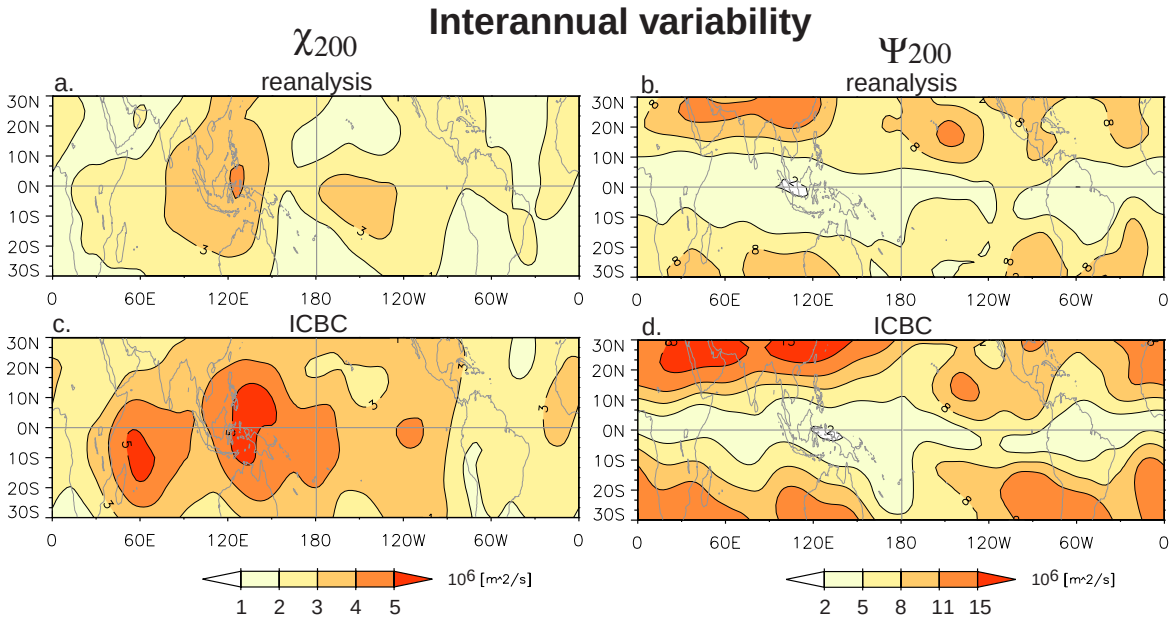

Fig. 4: Interannual standard deviation of January monthly mean velocity potential χ (left) and stream function ψ (right) at the 200 hPa level from NCEP/NCAR reanalysis (top) and model simulation ICBC (bottom). The base period is 1979-2000. Units are 10^6 m^2s^{-1}.

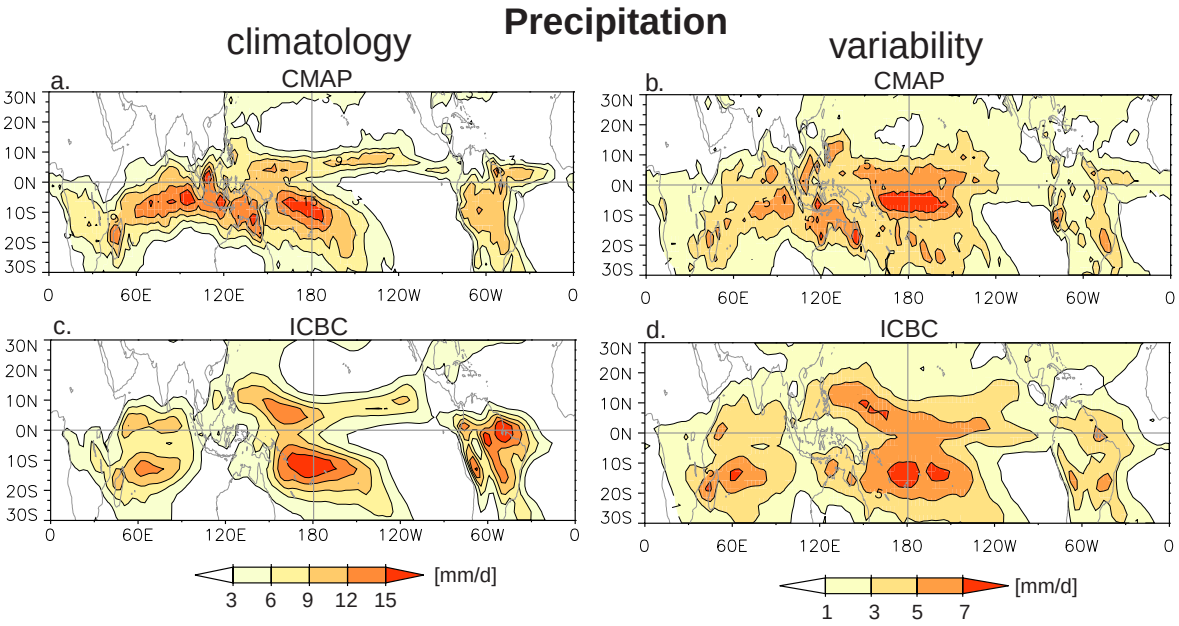

Fig. 5: Climatology (left panels) and interannual standard deviation (right panels) of January monthly mean precipitation from CMAP (top) and model simulation ICBC (bottom). The base period is 1979-2000. Units are mm/d.

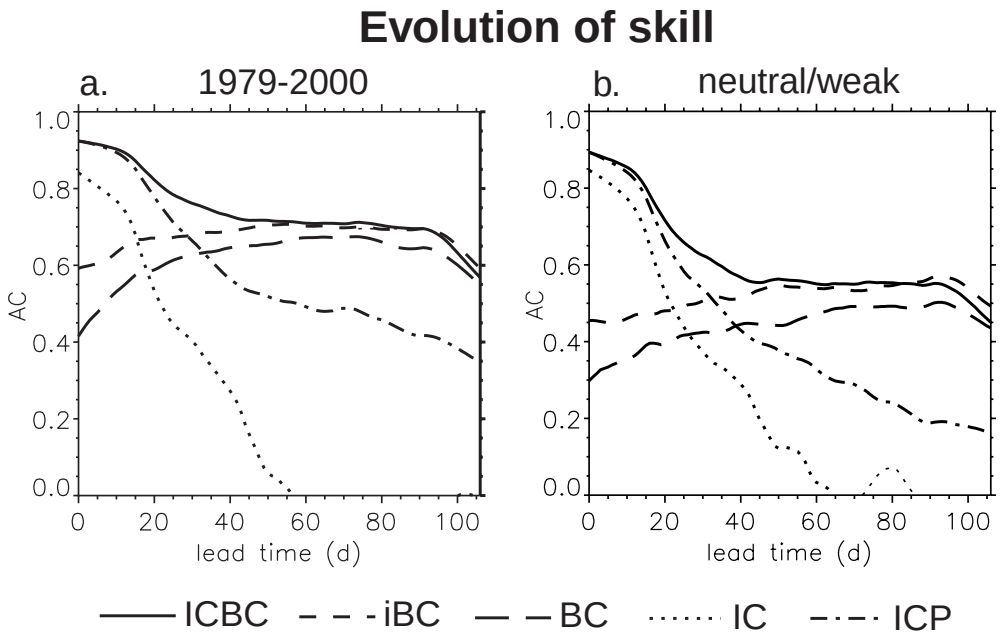

Fig. 6: Lead time evolution of spatial anomaly correlation from low-pass filtered equatorial χ_{200} (10ºN to 10ºS). (a) shows averages over all years, and (b) shows averages over neutral to weak ENSO years. Vertical axis denotes correlation. See Table 1 for definitions of ICBC, iBC, BC, IC and ICP.

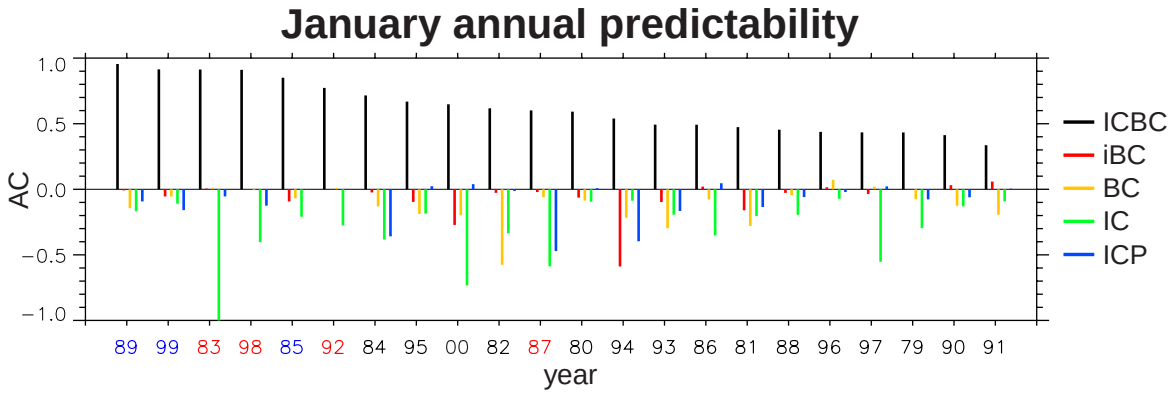

Fig. 7: Interannual variations of spatial anomaly correlations during January, derived from monthly mean equatorial χ_{200} (10ºN to 10ºS). Results for ICBC show absolute correlations, and other experiments show differences to ICBC. Cold (warm) ENSO years are shown by blue (red) year numbers. Vertical axis denotes correlation.

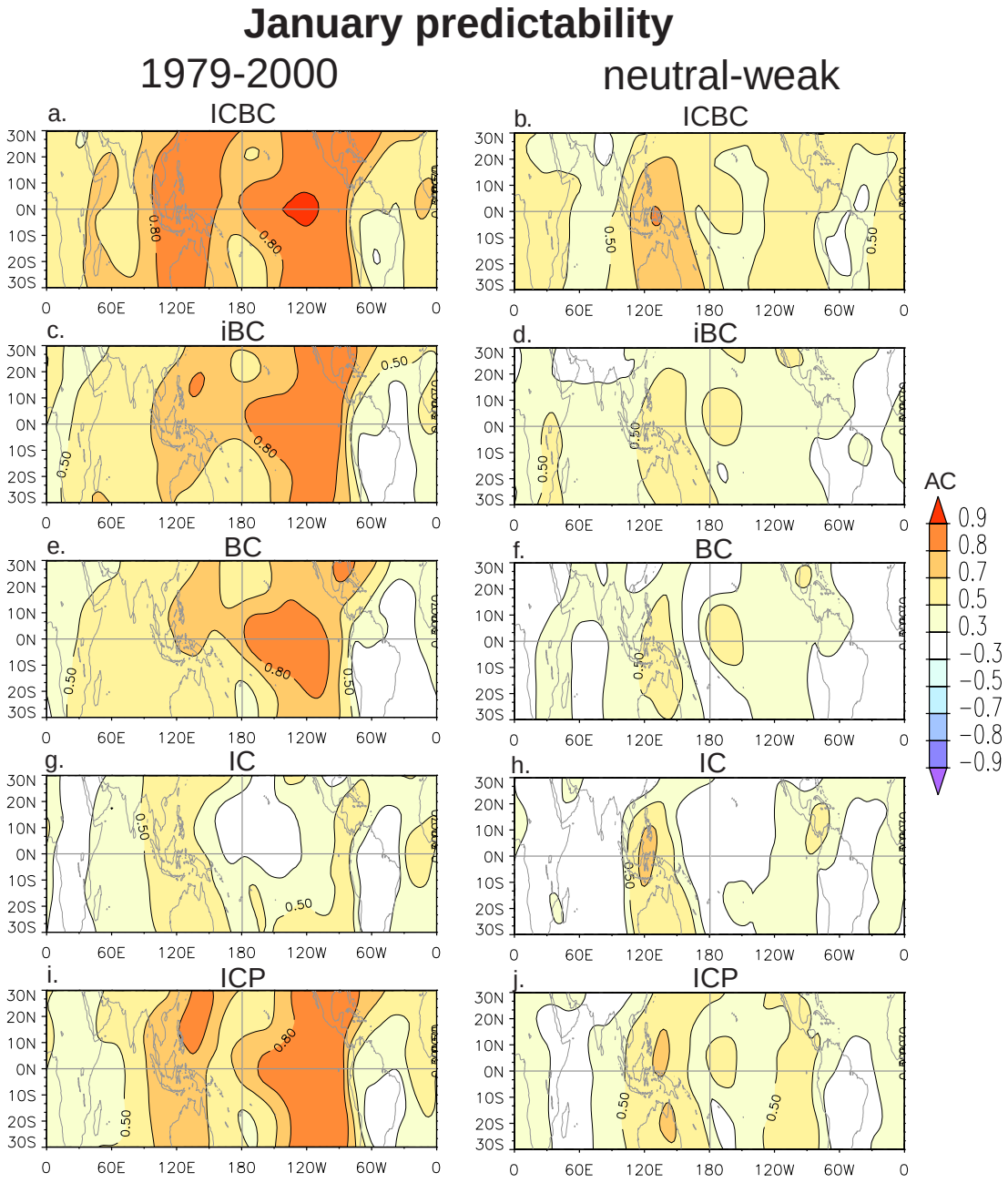

Fig. 8: Temporal anomaly correlations of January mean χ_{200} assuming perfect model. Left panels are for all 22 years from 1979-2000, and right panels are for neutral to weak ENSO years. See Table 1 for definitions of ICBC, iBC, BC, IC and ICP.

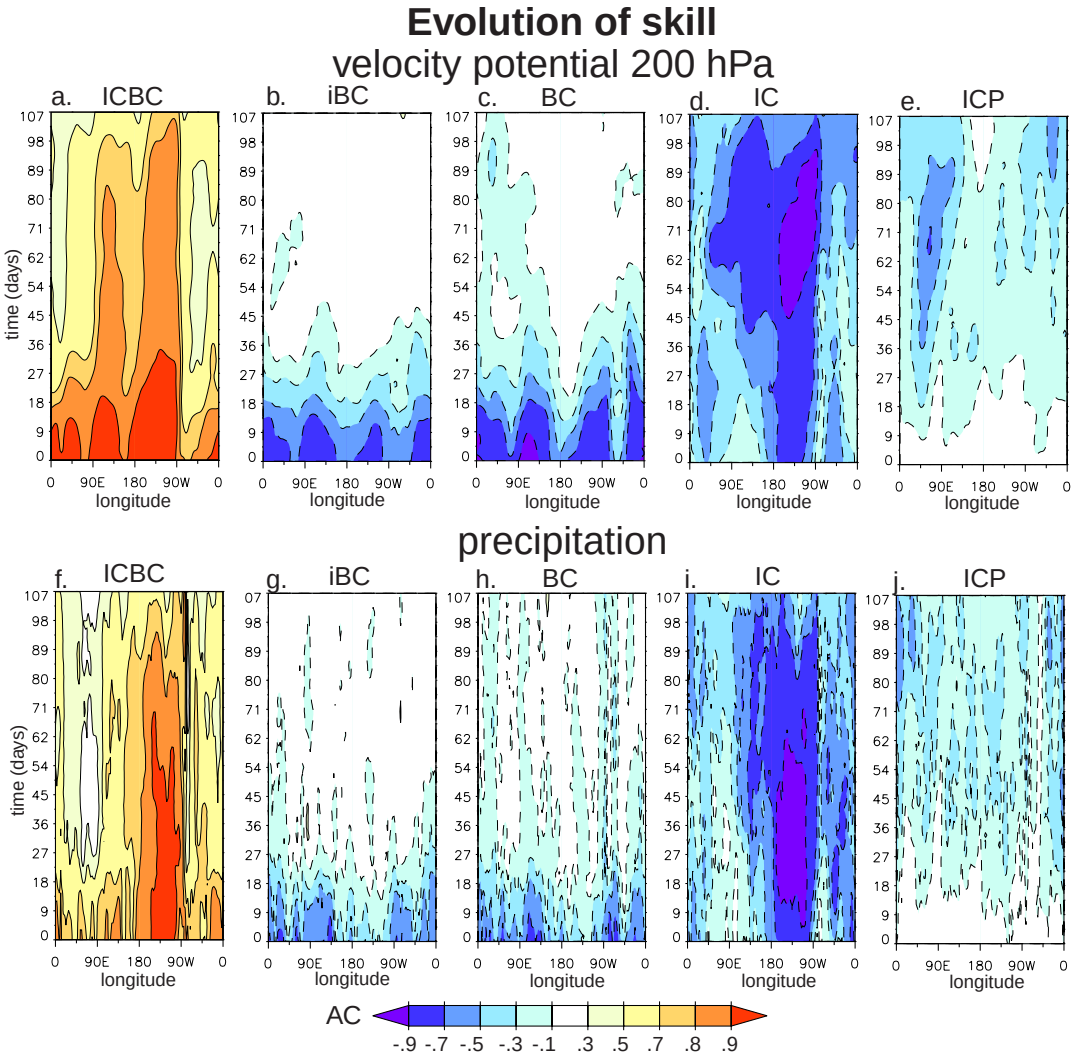

Fig. 9: Hovmöller diagram of temporal anomaly correlation (1979-2000) of monthly mean data along the equator (10°N-10°S). Top panels are for χ_{200}, and bottom panels are for precipitation. ICBC shows absolute correlations, and the other experiments show differences with respect to the ICBC. See Table 1 for definitions of ICBC, iBC, BC, IC and ICP.

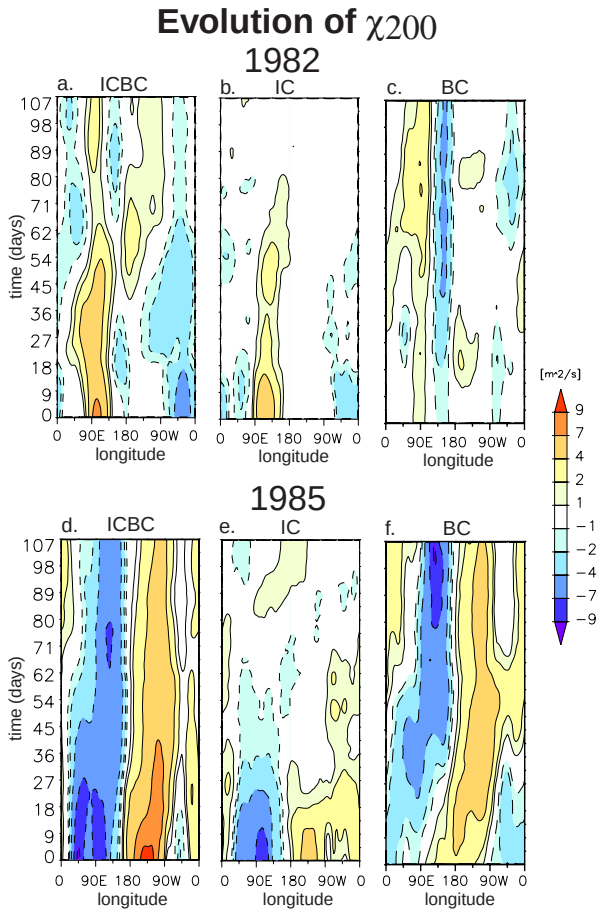

Fig. 10: Temporal evolution of low-pass filtered χ_{200} during winter 1982 (top) and 1985 (bottom). Shown are ensemble mean anomalies along the equator (10°N-10°S) from simulation ICBC (left), IC (middle), and BC (right). Units are 10^6 m^2s^{-1}.

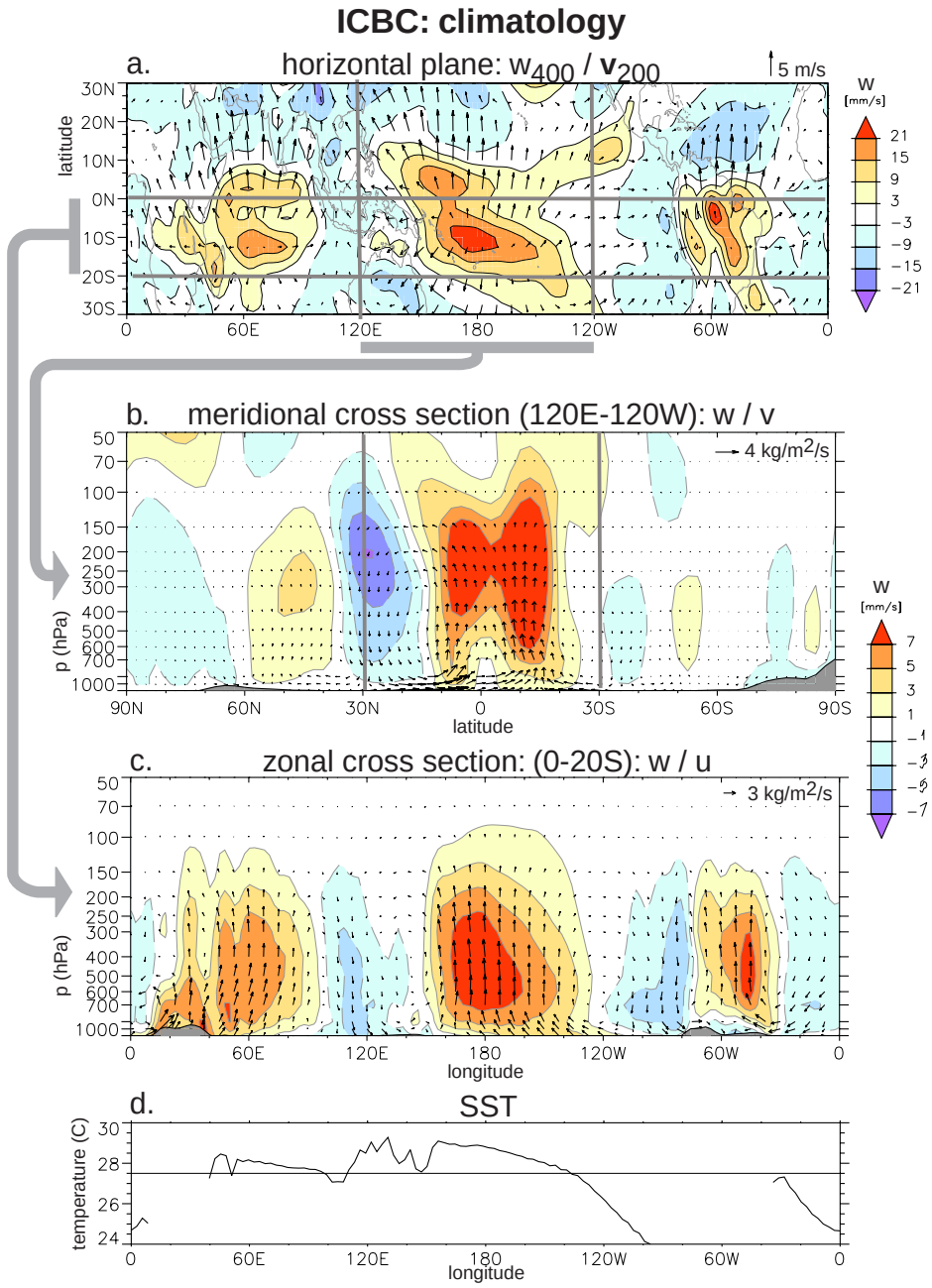

Fig. 11: Climatological mean (1979-2000) divergent circulation of simulation ICBC during January. Contours show vertical velocity in mm/s, and vectors show mass flux in kg m^{-2} s^{-1}. Shown are vertical velocity at 400 hPa and mass flux at 200 hPa in the XY-plane (top), zonal averages from 120°E-120°W in the YZ-plane (top-middle), meridional averages from 0-20°S along the equator (bottom-middle) and associated SSTs in °C (bottom). The cross sections use pressure in hPa as vertical coordinate (y-axis).

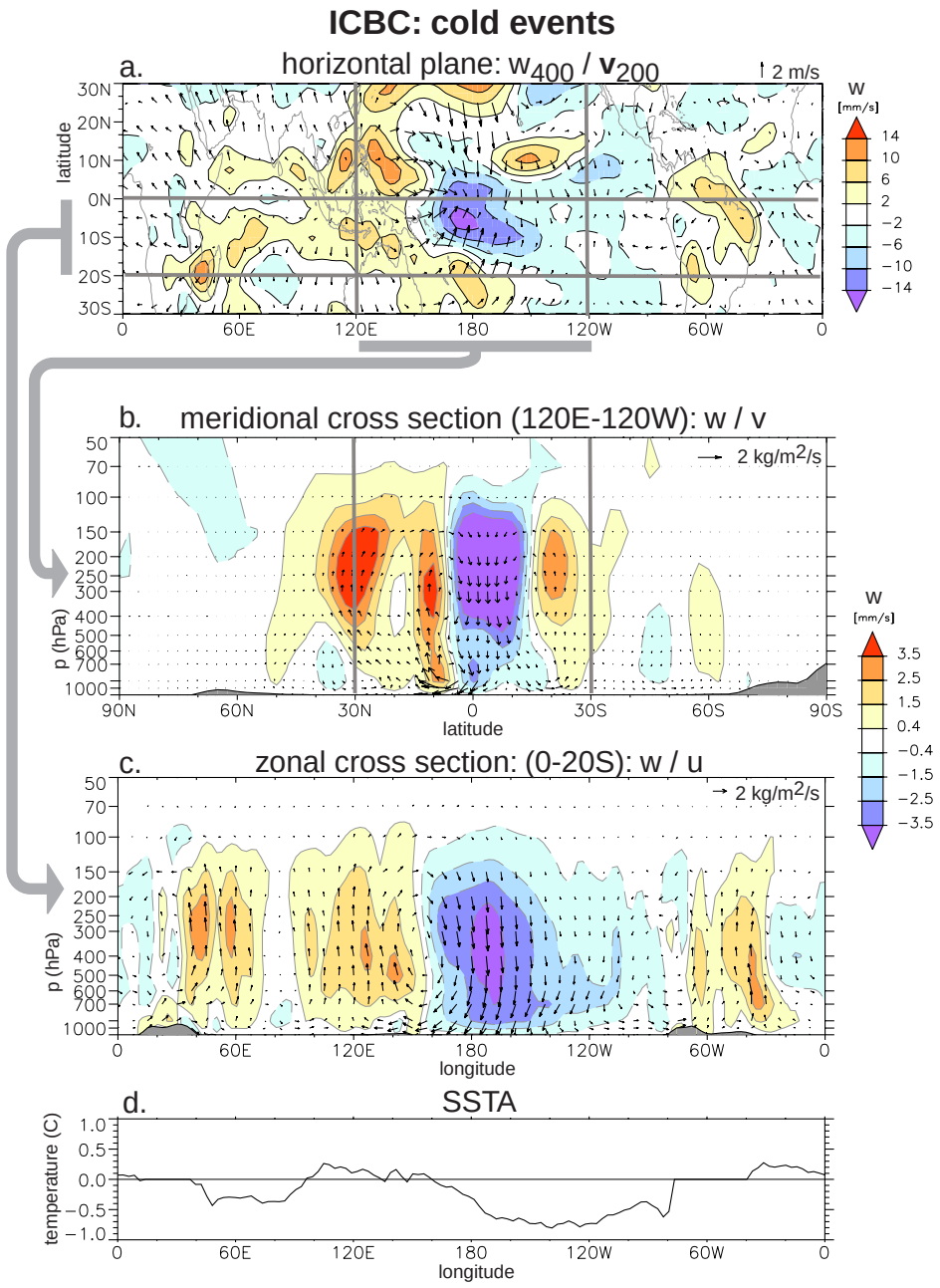

Fig. 12: As Fig. 11 but composite anomalies of 1985, 1989 and 1998 for simulation ICBC.

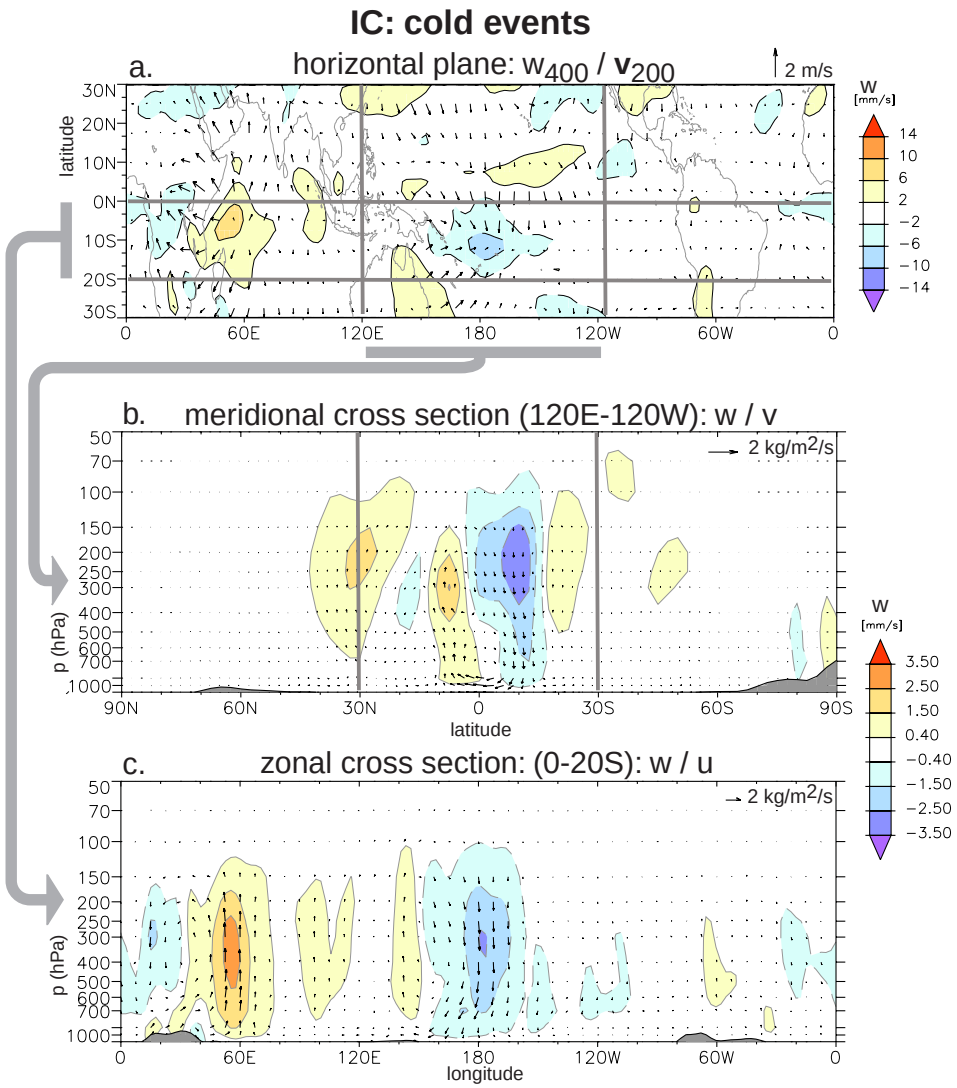

Fig. 13: As Fig. 11 but for simulation IC.

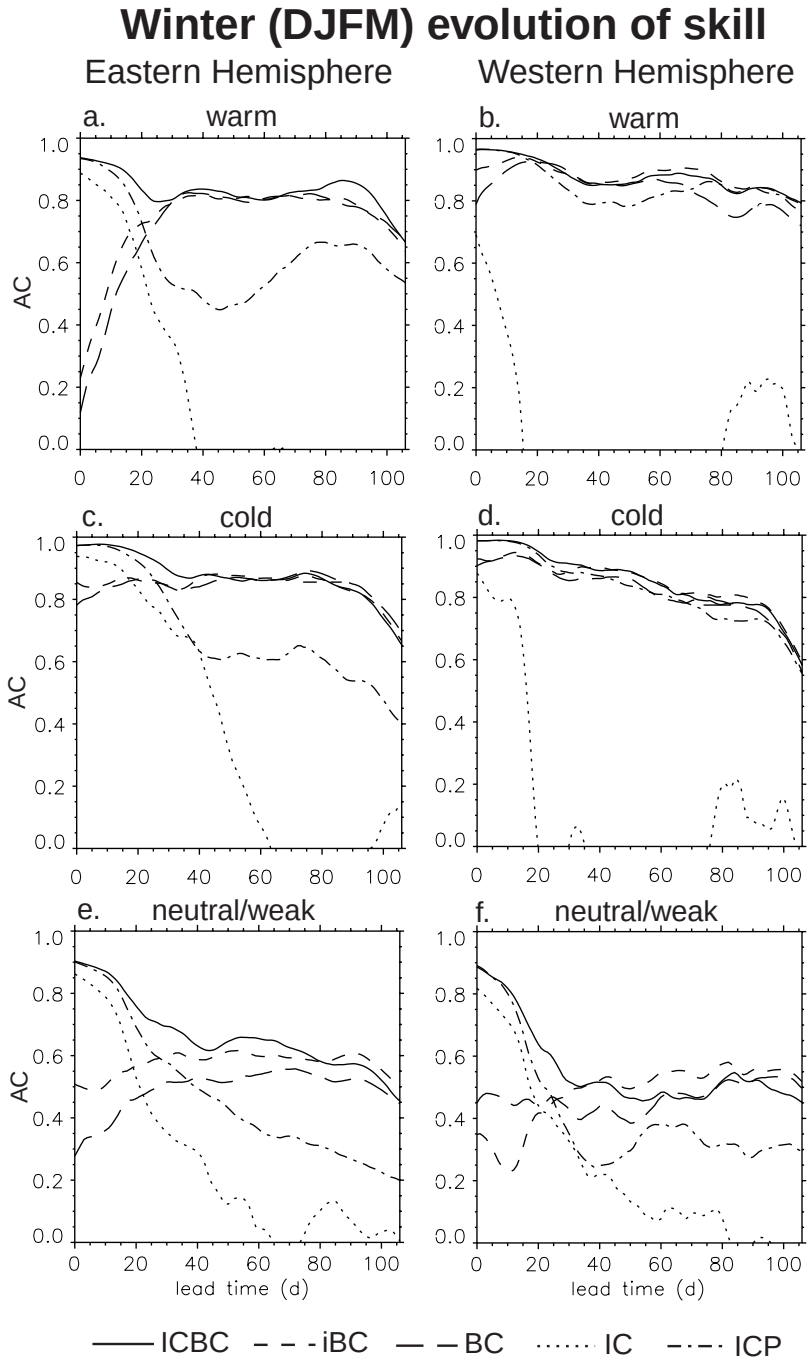

Fig. 14: Lead time evolution of spatial *AC*s of χ_{200} along the equator (10ºN to 10ºS), calculated separately for the eastern (0-180º) (left) and western (180º-360º) (right) hemisphere, and for warm (top), cold (middle) and neutral to weak ENSO years (bottom). See Table 1 for definitions of ICBC, iBC, BC, IC and ICP.

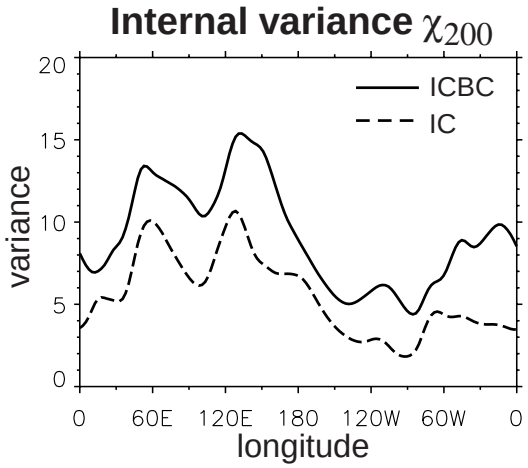

Fig. 15: Internal variability of filtered χ_{200} (10°N-10°S), averaged over day 40-106 and all 22 years (1979-2000). Units are 10^{12} m^4s^{-2}.

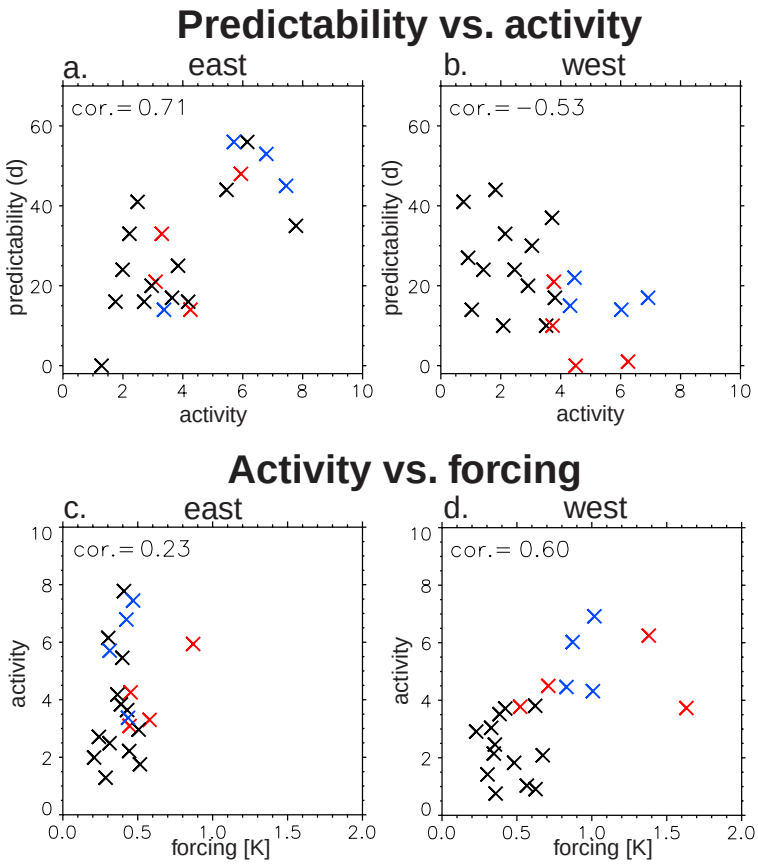

Fig. 16: Relationship between year to year variations in SST forcing (K), atmospheric activity (10^6 m^2s^{-1}), and initial condition predictability (days). Left panels are for eastern hemisphere (0º-180º), and right panels are for western hemisphere (180º-360º). Text in the upper left corner shows correlation between the quantities. Red (blue) x's indicate years with ENSO warm (cold) events.